



Coupling between gamma oscillation and fMRI signal in the rat somatosensory cortex: Its dependence on systemic physiological parameters

Akira Sumiyoshi^{a,*}, Hideaki Suzuki^b, Takeshi Ogawa^a, Jorge J. Riera^a, Hiroaki Shimokawa^b, Ryuta Kawashima^a

^a Department of Functional Brain Imaging, Institute of Development, Aging and Cancer, Tohoku University, Sendai, Japan

^b Department of Cardiovascular Medicine, Tohoku University Graduate School of Medicine, Sendai, Japan

ARTICLE INFO

Article history:

Received 3 September 2011

Revised 22 November 2011

Accepted 21 December 2011

Available online 8 January 2012

Keywords:

EEG–fMRI

Neurovascular coupling

Gamma oscillation

Baseline physiology

Small animal model

ABSTRACT

The simultaneous recordings of neuronal and hemodynamic signals have revealed a significant involvement of high frequency bands (e.g., gamma range, 25–70 Hz) in neurovascular coupling. However, the dependence on a physiological parameter is unknown. In this study, we performed simultaneous electroencephalography (EEG) and functional magnetic resonance imaging (fMRI) recordings in 12 Wistar rats using a conventional forepaw stimulation paradigm and concurrently monitored the systemic physiological parameters of the partial pressure of arterial oxygen, partial pressure of arterial carbon dioxide, pH, mean arterial blood pressure, and heart rate through the rat femoral artery. The high frequency bands in the artifact-free EEG signals, especially those in the gamma range, demonstrated a maximum correlation with fMRI signals in the rat somatosensory cortex. A multiple linear regression analysis demonstrated that the correlation coefficient between the gamma power and fMRI signal depended on the actual values of the physiological parameters ($R^2 = 0.20$, $p < 0.05$), whereas the gamma power and fMRI signal by itself were independent. Among the parameters, the heart rate had a statistically significant slope (95% CI: 0.00027–0.0016, $p < 0.01$) in a multiple linear regression model. These results indicate that neurovascular coupling is mainly driven by gamma oscillations, as expected, but coupling or potential decoupling is strongly influenced by systemic physiological parameters, which dynamically reflect the baseline vital status of the subject.

© 2012 Elsevier Inc. All rights reserved.

Introduction

Functional magnetic resonance imaging (fMRI) has replaced electroencephalography (EEG) and positron emission tomography as the central research tool in cognitive neuroscience (Friston, 2009). Although fMRI allows human brain functions to be investigated noninvasively, “fMRI signal interpretation” is still a major concern in the neuroimaging research community (Bandettini, 2009). fMRI is the indirect consequence of neuronal activity and is observed through alterations in blood flow, blood volume, or oxygen metabolism (Buxton, 2002). Therefore, it is important to gain further insights into the relationship between hemodynamic responses and underlying neuronal activity (Logothetis, 2008).

To address the aforementioned issue, simultaneous recordings of direct neuronal activity (i.e., EEG or intra-cranial recordings) and hemodynamic responses (i.e., fMRI or optical imaging) have been attempted for over a decade despite technical difficulties (Villringer et al., 2010). For example, Logothetis et al. (2001) demonstrated that fMRI signals reflect changes in local field potentials rather than

in spiking activity in the visual cortex of monkeys. Niessing et al. (2005) reported that 610 nm hemodynamic responses positively correlated with neuronal synchronization in the gamma range in the visual cortex of cats. More recently, such gamma band-specific positive correlations have been reproduced in humans performing a cognitive visual attention task (Scheeringa et al., 2011). These results and others (Goense and Logothetis, 2008; He et al., 2008; Lachaux et al., 2007; Mukamel et al., 2005; Nir et al., 2007; Schölvinck et al., 2010; Viswanathan and Freeman, 2007) have consistently indicated the significant involvement of gamma oscillations in neurovascular coupling across species and brain regions. The neurological origin and functional relevance of gamma oscillations have been extensively studied (Cardin et al., 2009; Sohal et al., 2009; Traub et al., 1996), yet it is still unclear why gamma oscillations preferentially correlate with hemodynamic responses (Riera and Sumiyoshi, 2010).

In addition to the neurogenic basis of neurovascular coupling, a number of studies indicate that fMRI signals are highly sensitive to physiological and/or pharmacological interventions, such as hypo/hyperoxia (Chiarelli et al., 2007; Sicard and Duong, 2005; Wibral et al., 2007), hypo/hypercapnia (Corfield et al., 2001; Posse et al., 2001; Zappe et al., 2008), hypo/hypertension (Masamoto et al., 2008; Qiao et al., 2007), hemodilution (Levin et al., 2001; Lin et al., 1998), and different anesthetics (Franceschini et al., 2010; Huttunen

* Corresponding author at: Institute of Development, Aging and Cancer, Tohoku University, Seiryō-machi 4-1, Aoba-ku, Sendai 980-8575, Japan. Fax: +81 22 717 8468.

E-mail address: sumiyoshi@idac.tohoku.ac.jp (A. Sumiyoshi).

et al., 2008; Smith et al., 2002). These findings highlight the importance of the basal condition in evoked fMRI responses and suggest that we take caution when interpreting the fMRI signals of subjects whose physiological parameters may differ. It is standard procedure that fMRI researchers, especially those using anesthetized animal models (e.g., rat: Hyder et al., 1994; cat: Jezzard et al., 1997; monkey: Logothetis et al., 1999), report the systemic physiological parameters of their subjects, such as the partial pressure of arterial oxygen (PaO₂), partial pressure of arterial carbon dioxide (PaCO₂), pH, mean arterial blood pressure (MABP), and heart rate (HR), to verify their results and conclusions (Steward et al., 2005). However, the perturbations in neuronal responses caused by such experimental interventions are not directly or simultaneously evaluated in most cases. Thus, it is difficult to conclude whether the changes in fMRI signals are derived from neuronal and/or hemodynamic consequences. Normally, it is difficult to extrapolate findings into cognitive fMRI research because the physiological parameters evaluated during experimental interventions are far above/below the ranges that are normally assumed for healthy human subjects.

We also investigate the influence of baseline physiology on neurovascular coupling in this study. More specifically, we report on the trial-by-trial relationship between EEG responses in each frequency band and fMRI signals and their dependence on the physiological parameters within a normal physiological range. To achieve this, we repeatedly performed simultaneous EEG and fMRI recordings in 12 α -chloralose anesthetized rats as previously described (Sumiyoshi et al., 2011). In addition, we achieved concurrent physiological monitoring of several systemic parameters (i.e., PaO₂, PaCO₂, pH, MABP, and HR) through the rat femoral artery during simultaneous EEG–fMRI acquisitions. To reduce artifact in the EEG data, an independent component analysis (ICA) method (Mantini et al., 2007a) was successfully applied. Finally, we examined the correlation coefficients between the powers of the EEG in each frequency band and the fMRI signals in the rat somatosensory cortex and performed a multiple linear regression analysis to statistically elucidate the impact of the physiological parameters on neurovascular coupling.

Materials and methods

Animal preparation

The experiments were conducted on 12 male Wistar rats, weighing 206 ± 12 g (Charles River, Yokohama, Japan). All procedures were performed in agreement with the policies established by the Animal Care Committee at Tohoku University (approval code, 2011AcA-40). Each rat was initially anesthetized with isoflurane (5% for the initial induction and 3% during surgery). The scalp hair was carefully removed with an electric shaver and a medical razor. The exposed skin was de-greased with 70% ethanol. The tail vein was catheterized using a 24 G plastic cannula for systemic and continuous drug delivery through a syringe pump (TOP-5300, TOP, Tokyo, Japan). Each rat was orally intubated with a 16 G plastic cannula and mechanically ventilated (the inspired gas was a mixture of 40% O₂ and 60% N₂) at approximately 60 breaths per minute (BPM) using a small animal ventilator (SAR-830/AP, CWE Inc., Ardmore, PA, USA). The rats were administered a muscle relaxing agent (pancuronium bromide, 2.0 mg/kg/h i.v.). After surgery, each rat was placed in the prone position on a custom-built MRI-bed with a bite bar, and the anesthetic was switched from isoflurane to α -chloralose (80 mg/kg as an initial bolus, followed by a constant infusion of 26.7 mg/kg/h). The temperature was monitored using an MRI-compatible temperature probe (Model 1025, SA Instruments, Stony Brook, NY, USA) inserted into the rectum. The core body temperature was carefully regulated during the entire experiment by means of a heated water-circulating pad. A pair of small needle electrodes (NE-224S, Nihon

Kohden, Tokyo, Japan) was inserted under the skin of either the right or left forepaw for electrical stimulation.

Arterial blood gas/pressure monitoring

The left femoral artery was approached from the left inguinal region of the rats. The artery was clearly dissociated from the nerve and the vein. The distal portion of the artery was tied with a 4-0 silk string, and the proximal portion was clamped with forceps. A tiny hole was made in the arterial wall with micro-scissors, and a polyethylene catheter (inner diameter: 0.5 mm and outer diameter: 0.8 mm) filled with 100 U/ml heparinized saline solution was inserted into the hole. The arterial wall and the catheter were fixed with a 4-0 silk string and liquid glue (Vetbond™, 3M Animal Care Products, St. Paul, MN, USA). The clamp was released, and the lumen of the catheter was flushed with 100 U/ml heparinized saline solution. The procedure was confirmed by observing the backflow of arterial blood inside the catheter. The arterial blood pressure was digitized by DTXPlus™ (BD, Franklin Lakes, NJ, USA) connected to the polyethylene catheter, amplified by MEG-6108 (Nihon Kohden, Tokyo, Japan) and analyzed by PowerLab/16SP and LabChart 6 (ADInstruments, Colorado Springs, CO, USA). The MABP and HR were obtained from an average of 60 s of digitized data. Meanwhile, the blood gas sampling was performed as follows. First, the heparinized saline solution inside the lumen of the left femoral catheter was removed. Second, approximately 0.3 ml of blood from the catheter was extracted using a 1.0 ml heparin-coated syringe. Third, the removed saline solution was returned to the catheter, and the lumen of the catheter was flushed with 100 U/ml heparinized saline solution. Finally, the extracted blood was analyzed by a Rapidlab 248 blood gas analyzer (Siemens, Munich, Germany) to obtain the values of PaO₂, PaCO₂, and pH. Thus, the MABP and HR were continuously monitored throughout the experiment, and the PaO₂, PaCO₂, and pH were obtained in a discontinuous manner.

Electrophysiological recordings: EEG and ECG

For simultaneous EEG and fMRI data acquisition, we prepared an EEG mini-cap that was compatible with MRI and was specifically designed for rodents. The details of the rodent EEG mini-cap, such as the design, material, and recording principle, were described in a previous study (Sumiyoshi et al., 2011). In brief, the mini-cap is composed of a total of 31 EEG electrodes made of platinum wires (PT-351325, Nilaco, Tokyo, Japan) that were placed on the rat scalp with an inter-electrode distance of 3.0 mm. Each electrode was immersed in a highly conductive EEG paste (0.81 S/m at 25 °C) and confined in a cylindrical silicon tube (diameter: 1.3 mm and length: 10 mm). The impedance of each electrode was maintained under 50 k Ω . The data were collected using a 32-channel MR-compatible BrainAmp system (Brain Products, Munich, Germany) with a sampling rate of 5 kHz. We applied band-pass-filtering from 0.5 to 250 Hz along with 50-Hz notch filtering. An additional channel was used to record the ECG through a needle (Model 1025, SA Instruments, Stony Brook, NY, USA) that was inserted into the right hindpaw. To synchronize the EEG data with fMRI scanning, analog outputs (5 V) generated by an MRI console were digitized (16-bit resolution) as triggers to the EEG amplifiers and were subsequently utilized for the offline removal of scanning artifacts. The reference and ground electrodes (NE-224S, Nihon Kohden, Tokyo, Japan) were subdermally inserted into the right and left earlobes, respectively.

MRI recordings: fMRI and T2

All of the MRI data were acquired using a 7.0-T Bruker PharmaScan system (Bruker Biospin, Ettlingen, Germany) with a 38 mm diameter

birdcage coil. Prior to all of the MRI experiments, the global magnetic field shimming was performed first inside the core and later completed at the region-of-interest (ROI) using a point-resolved spectroscopic protocol. The line width (full width at half maximum) at the end of the shimming procedure ranged from 15 to 20 Hz in the ROI (~300 μ l). The fMRI signals were obtained using the GE-EPI with the following parameters: TR = 2000 ms, TE = 15 ms, SBW = 250 kHz, flip angle = 30°, FOV = 25 × 14 mm², matrix size = 125 × 70, voxel size = 200 × 200 μ m², number of slices = 7, slice thickness = 1.5 mm, slice gap = 0 mm, number of volumes = 370, and dummy scans = 4. The T2-weighted anatomical images were obtained using the 2D-RARE sequence with the following parameters: TR = 4600 ms, TE_{eff} = 30 ms, RARE factor = 4, SBW = 100 kHz, flip angle = 90°, FOV = 32 × 32 mm², matrix size = 256 × 256, voxel size = 125 × 125 μ m², number of slices = 54, slice thickness = 0.5 mm, slice gap = 0 mm, and number of averages = 24. The iMagic and Brainbow software (Neuronic S.A., Havana, Cuba) were used for T2-weighted image data processing and visualization, respectively.

Experimental design

A simultaneous EEG–fMRI measurement consisting of a block-design stimulation paradigm and a subsequent blood gas sampling (approximately 0.3 ml in each blood sampling) was performed once every hour for 5 h after α -chloralose anesthesia induction. In this study, we are referring to the combination of an EEG–fMRI measurement and a blood gas sampling as an “experiment”. Thus, a total of 60 experiments (5 experiments per rat) were utilized for statistical analyses, and no exclusion criteria were considered. A block-design stimulation paradigm consisting of 10 blocks was employed, where each block comprised of a 30 s forepaw stimulation followed by a 40 s resting condition. A generator (SEN-3401, Nihon Kohden, Tokyo, Japan) and an isolator (SS-203J, Nihon Kohden, Tokyo, Japan) were utilized to produce the electrical pulses (3 Hz, 3 mA, and 0.3 ms width). Either the left or right forepaw was stimulated ($n = 6$ animals in each) to create a balance across all of the animals. No significant increase or decrease in the MABP was observed (within ± 2.0 mm Hg change in the mean). In addition to the experiment performed inside of the MRI scanner, the same block-design stimulation paradigm was also performed outside of the MRI scanner for a pair-based comparison of the quality of the EEG data.

EEG data analysis

The procedure for the EEG data analysis was based on the strategy described by Mantini et al. (2007a) for attenuating a wide variety of artifacts, which caused contamination due to the nature of the simultaneous EEG–fMRI acquisitions. Briefly, the Brain Vision Analyzer software (Brain Products, Munich, Germany) was used for the offline correction of fMRI scanning artifacts. This software implements the adaptive artifact subtraction (AAS) method, in which the scanning artifact waveforms are segmented (–10 ms to 276 ms relative to the scanning trigger), averaged (after baseline correction), and iteratively subtracted from the EEG signals. The data were then down-sampled to 1 kHz, band-pass-filtered from 0.5 to 70 Hz using a Butterworth filter with a 24 dB/oct slope and finally exported into a binary format (Supplementary Fig. 1A). The subsequent EEG data analysis was performed using custom-written software in MATLAB (MathWorks, Natick, MA, USA). To reject the ballisto-cardiogram (BCG) and other undesirable artifacts from the filtered EEG data, an ICA-based subtraction method was employed. The procedure for artifact reduction was as follows: first, the data were visually checked to exclude noisy EEG channels and re-referenced to the mean across all of the channels. Second, the ICA decomposition into the 30 source signals was performed by the FastICA algorithm (Supplementary Fig. 1B). Third, the classification of 30 source signals into artifacts was performed either

with a manual or an automated approach (e.g., Supplementary Fig. 2). Fourth, the IC components identified as artifacts were projected back on to the channel level and then subtracted from the filtered EEG data (Supplementary Fig. 3). The criteria we used for classifying the IC components were as follows: (1) for the BCG artifact, the correlation coefficient with the ECG is larger than 0.2; (2) for the respiration artifact, the power percentage of the sharp 1.0 Hz peak in the periodogram is larger than 1.0%; (3) for the occasional artifact, the maximum amplitude in the back-projected data is larger than 80 μ V. While (1) and (3) are exactly the same criteria that were previously used in the literature, (2) is a novel criterion because respiration is continuously controlled by mechanical ventilation at approximately 60 BPM in this study. The mean event-related potential (ERP) for each experiment was computed from 900 individual evoked potentials (–50 ms to 200 ms relative to the stimulus onset) after a baseline correction (–50 ms to 0 ms relative to the stimulus onset). Finally, the Euclidean distance was computed for pair-based comparisons of ERP waveforms.

fMRI data analysis

The fMRI data analysis was performed using SPM5 (Wellcome Department of Cognitive Neurology, London, UK) and custom-written software in MATLAB, which consisted of adjustments of the acquisition timing across slices, correction for head movement, and smoothing using a Gaussian kernel of 0.8 mm full width at half maximum. The single-subject analysis of the preprocessed fMRI data was performed using SPM5 with a critical T-value for each voxel ($p < 0.05$, FWE corrected). To further evaluate the fMRI results, an average time course within the spherical ROI (0.6 mm radius) centered on the highest T-scores was extracted. The drift was removed by subtracting the low-frequency components of its discrete cosine transform, and the time courses of the fMRI data were low-pass-filtered (6th order Butterworth filter, <0.1 Hz). The statistical T-scores of the fMRI data were computed by the MarsBaR toolbox (<http://marsbar.sourceforge.net/>) using the conventional hemodynamic response function (HRF).

Neurovascular coupling data analysis

To quantify the trial-by-trial relationship between the EEG and fMRI data, Pearson's correlation coefficients were calculated for each experiment. First, the electrode located most proximal to the fMRI activation site and exhibiting the highest response in terms of ERP magnitude was carefully selected. Second, the EEG data from the selected electrode was band-pass-filtered (delta: 1–4 Hz, theta: 4–8 Hz, alpha: 8–12 Hz, beta: 12–25 Hz, and gamma: 25–70 Hz) and the power of each frequency band was averaged in epochs of 2000 ms, which corresponded with the TR of fMRI acquisition. Third, they were convolved with a canonical HRF in SPM5 (delay of response = 6; delay of undershoot = 16; dispersion of response = 1; dispersion of undershoot = 1; ratio of response to undershoot = 6; onset = 0; length of kernel = 32). Fourth, after removing the first and last 10 points of the data, Pearson's correlation coefficients between the EEG (in each frequency band) and fMRI data, which served as an indicator of neurovascular coupling, were computed for each experiment. The statistical T-scores of the EEG data in each frequency band were computed in parallel after HRF convolution using the MarsBaR software, which is similar to the scoring procedure used in the fMRI data analysis.

Multiple linear regression analysis

A multiple linear regression model was applied to relate the outcome of the simultaneous EEG–fMRI measurement to the physiological parameters of PaO₂, PaCO₂, pH, MABP, and HR, which were concurrently

obtained in each experiment. The multiple linear regression model tested in this study is shown below.

$$Y_{data} = \beta_0 + \beta_{PaO_2} \times X_{PaO_2} + \beta_{PaCO_2} \times X_{PaCO_2} + \beta_{pH} \times X_{pH} + \beta_{MABP} \times X_{MABP} + \beta_{HR} \times X_{HR} + \varepsilon$$

where Y_{data} represents the correlation coefficient or the EEG/fMRI T-score, β_0 represents the intercept, β_{PaO_2} , β_{PaCO_2} , β_{pH} , β_{MABP} , and β_{HR} represent the slope for each regressor, X_{PaO_2} , X_{PaCO_2} , X_{pH} , X_{MABP} , and X_{HR} represent the actual data of each physiological parameter, and ε represents the error term. The regression model yielded an R -squared value, an indicator of the fitness of the regression models. A significance level of 0.05 was used, and a 95% confidence interval (95% CI) was calculated for each regression slope.

Results

Signal quality of the EEG and fMRI data

A representative result of a simultaneous EEG–fMRI recording in an individual rat is shown in Fig. 1A. The fMRI signal shows significant event-related responses using the unilateral forepaw stimulation paradigm. After the artifact reduction in the EEG signal, the ERPs can be appreciated even on a single-trial basis (Fig. 1B). Note that the EEG signal is derived from a single electrode located most proximal to the fMRI activation site in the somatosensory cortex (Fig. 1C and D).

The differences in the ERP waveform were compared to exemplify the performance of the ICA method. An example of the ERP obtained from recordings made outside and inside of the MRI scanner is depicted in Fig. 2. Although the amplitude and waveform of the ERPs were similar across all of the conditions, the standard deviation was only moderately decreased after AAS + ICA processing. These results were reproduced in each rat with little inter-subject variability (Table 1). Additionally, the reduction of the noise level in the EEG data after AAS + ICA processing was confirmed by comparing the 50 ms pre-stimulus baseline across all of the conditions (Table 2).

Correlation between the EEG signal in each frequency band and the fMRI signal

The time course of the EEG signal in each frequency band of an individual rat, after down-sampling to TR (black) and convolution with an HRF (red), are shown in Fig. 3. In addition, the fMRI signal can also be observed at the bottom of Fig. 3. To investigate the differences among the frequency bands, Pearson's correlation coefficients between the EEG and fMRI signals were calculated for all of the frequency bands (Fig. 4A). The higher frequency bands of alpha, beta and gamma demonstrate a higher and more significant correlation with fMRI signals, whereas the lower frequency bands, such as delta and theta, demonstrate a lower correlation with relatively high variability. Not all of the p -values for the lower frequency bands were less than 0.05 (e.g., 32% of delta and 10% of theta were more than 0.05), whereas all of the p -values for the higher frequency bands were less than 0.0001. The significant correlations in the higher frequency bands could be interpreted in relation to the higher signal-to-noise ratio of the EEG responses, as shown in Fig. 4B.

Physiological parameters during simultaneous EEG–fMRI acquisition

The systemic physiological parameters across all of the experiments were as follows: PaO_2 , 114 ± 16 mm Hg (86–161 mm Hg); $PaCO_2$, 38.8 ± 7.3 mm Hg (23.5–56.3 mm Hg); pH, 7.34 ± 0.04 (7.24–7.45); MABP, 105 ± 17 mm Hg (66–141 mm Hg); and HR, 467 ± 44 beats/min (376–571 beats/min). The distribution of the five systemic physiological parameters, which were utilized for the subsequent multiple linear regression analysis, is shown in Fig. 5. The body temperature was 35.9 ± 0.6 °C (34.7–37.0 °C) across all of the experiments. This is a slightly lower range than what is typically observed in a rat fMRI study. However, we did not find any significant correlation between the body temperature and other variables (Supplementary Table 1), which indicates that there is negligible influence of body temperature on the five systemic physiological parameters and the quantities derived from the EEG and fMRI signals.

Influence of physiological parameters on neurovascular coupling

A multiple linear regression analysis was performed to investigate the influence of PaO_2 , $PaCO_2$, pH, MABP, and HR on the EEG/fMRI T-

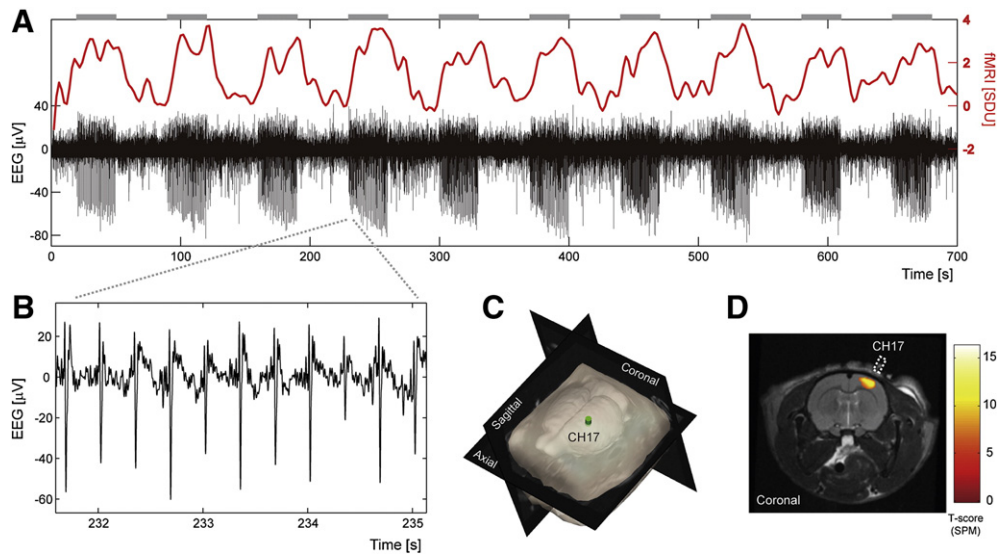


Fig. 1. (A) A representative example of a simultaneous EEG and fMRI recording in an individual rat. The black line denotes the EEG signal (from one channel) and the red line denotes the fMRI signal, respectively. The gray horizontal bar indicates the unilateral forepaw stimulation period. (B) An amplified image of the EEG data. (C) The scalp and brain surfaces of the rat. The green cylindrical object shows the position of the electrode (same channel as above). (D) The selected electrode is located most proximal to the fMRI activation site. The SPM t -test score ($p < 0.05$, FWE corrected) is co-registered on the individual T2-weighted anatomical image.

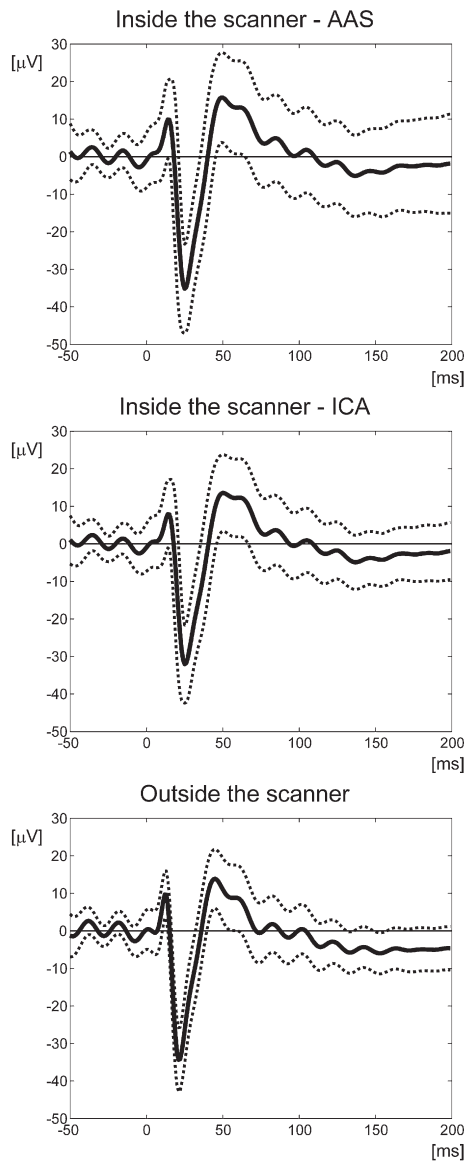


Fig. 2. ERPs (solid line) after artifact reduction using the AAS method (top), after processing using both the AAS and ICA methods (middle), and the ERP recorded outside of the MRI scanner (bottom) from the same rat are shown with the standard deviation (dashed line).

Table 1
Differences in the ERP signal waveforms (μV).

	Outside vs. inside (AAS)		Outside vs. inside (ICA)	
	Mean	Std	Mean	Std
Rat #1	0.416	0.135	0.277	0.100
Rat #2	0.259	0.097	0.233	0.095
Rat #3	0.168	0.072	0.148	0.072
Rat #4	0.234	0.097	0.200	0.086
Rat #5	0.248	0.089	0.242	0.087
Rat #6	0.360	0.126	0.287	0.110
Rat #7	0.113	0.037	0.105	0.036
Rat #8	0.213	0.084	0.173	0.060
Rat #9	0.211	0.075	0.164	0.051
Rat #10	0.212	0.078	0.178	0.056
Rat #11	0.264	0.147	0.219	0.089
Rat #12	0.132	0.068	0.115	0.063
Group	0.236 ^a	0.092	0.195 ^a	0.075

For each animal, the mean value and standard deviation (Std) from all of the recording channels were calculated through pair-based comparison. The group statistics are also shown at the bottom of the table (Student's *t*-test, $p = 0.0024^a$).

Table 2
Standard deviation of 50 ms pre-stimulus baseline (μV).

	Inside (AAS)		Inside (ICA)		Outside	
	Mean	Std	Mean	Std	Mean	Std
Rat #1	9.747	1.913	6.524	0.991	6.774	1.619
Rat #2	7.904	3.383	4.994	1.002	4.866	1.262
Rat #3	8.324	1.311	7.271	1.656	5.590	1.177
Rat #4	7.328	1.642	5.481	1.691	4.911	1.371
Rat #5	8.285	2.965	6.470	1.372	6.703	1.571
Rat #6	6.888	1.263	4.683	0.883	3.722	0.732
Rat #7	5.858	1.427	4.451	1.358	4.156	1.140
Rat #8	6.496	1.112	5.322	1.116	5.540	1.432
Rat #9	6.675	2.309	3.722	0.850	2.182	0.891
Rat #10	7.713	1.340	6.110	1.389	7.205	1.889
Rat #11	6.413	2.722	3.997	1.334	5.210	1.586
Rat #12	9.404	3.240	3.977	1.309	2.692	0.609
Group	7.586 ^a	2.052	5.250 ^{a, b}	1.246	4.963 ^b	1.273

The mean value and standard deviation (Std) from all of the recording channels were computed for each animal. The values refer to the overall noise level in the EEG data. The group statistics are also shown at the bottom of the table (ANOVA with multiple comparisons, $p < 0.05^a$, $p > 0.05^b$).

score or correlation coefficient (Table 3). The correlation coefficients between several frequency bands and fMRI signals were dependent on the actual values of the five physiological parameters ($p < 0.05$). The EEG T-scores of the delta and theta frequency bands were also fitted by the five physiological parameters ($p < 0.05$). Therefore, there is a possibility that the linear regression model of the correlation coefficient in these bands was influenced by the high dependency of both EEG bands on the five physiological parameters. However, both the EEG T-scores in the gamma frequency bands and the fMRI T-scores were entirely independent of the five physiological parameters.

The details of the multiple linear regression model of the correlation coefficient between the gamma frequency band and the fMRI signal are shown in Table 4. Only the HR exhibited a statistically significant positive slope ($p < 0.05$), while the other regressors demonstrated a slope at the 95% CI, shifting from a negative to a positive value. However, both the pH and MABP approached significance at $p = 0.06$ and 0.07 , respectively. Thus, the five physiological parameters demonstrated distinct influences on the coupling between gamma oscillations and fMRI signals.

Discussion

Artifact reduction by the ICA-based method

Various groups have proposed the use of the ICA-based noise reduction method in simultaneous EEG–fMRI studies over the last decade (Béнар et al., 2003; Debener et al., 2010; Nakamura et al., 2006; Srivastava et al., 2005). ICA is a signal processing algorithm that has been used to statistically separate complex multichannel EEG data into IC components without requiring detailed models of either the dynamics or the spatial structure of the separated components (Jung et al., 2001). Thus, the ICA method offers a distinct advantage over the classical method because the BCG and other artifacts (e.g., ocular artifacts and residual scanning artifact) can be concurrently identified and eliminated. Therefore, we employed the ICA method previously described by Mantini et al. (2007a) and its validation protocols in this study, and we successfully demonstrated its applicability to small animal EEG–fMRI studies. Consistent with other studies, the ICA method provides quality EEG or ERP data that is comparable with that obtained from outside of the MRI scanner (Tables 1 and 2). We believe that the reduction of the BCG, respiration, and other occasional artifacts is equally important. Thus, the ICA method is the most suitable technique for small animal EEG–fMRI studies. Here, we note that the performance of noise reduction is largely

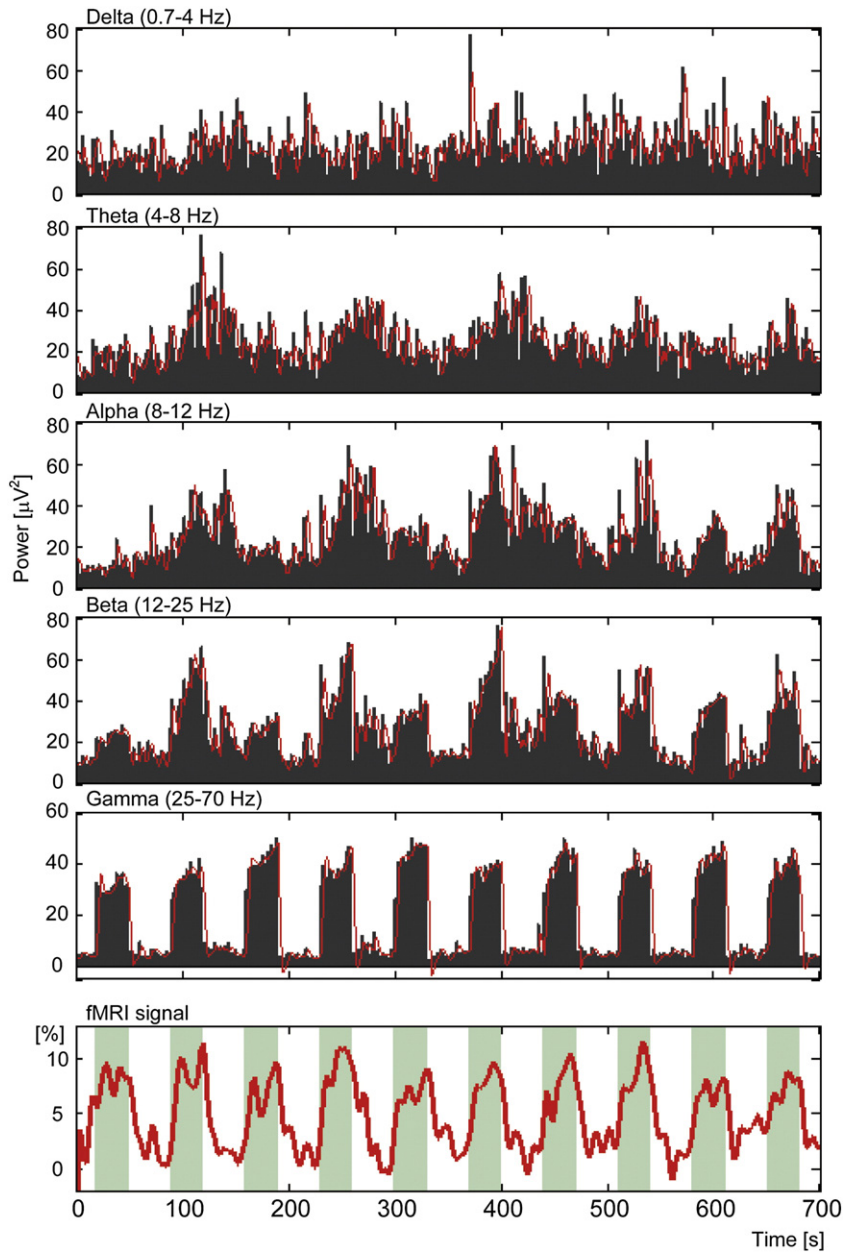


Fig. 3. An illustrative example of the EEG data analysis. The power (black) in each frequency band is convolved with an HRF and used as a regressor (red) for the subsequent correlation analysis. The green shading indicates the times when the stimulus was applied.

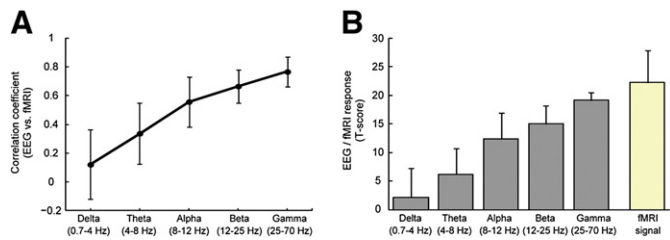


Fig. 4. (A) The statistical T-scores of the EEG data in each frequency band (gray bar) and fMRI data (yellow bar) across all of the animals ($n = 12$) with the standard deviation. The high frequency bands in the EEG data demonstrate a robust event-related response under the unilateral forepaw stimulation paradigm. (B) Correlation coefficients between the EEG in each frequency band and fMRI across all of the animals ($n = 12$) with the standard deviation. The high frequency bands, especially those in gamma range, demonstrate a significant correlation with the fMRI signals and exhibit less standard deviation.

dependent on the data pre-processing, which consists of the removal of noisy channels, data filtering, and even the performance of a principal component analysis prior to ICA, as suggested by Vanderperren et al. (2010). The selection criteria for noise IC components should also be carefully considered on a case-by-case basis, taking into account the particulars of the animal preparation protocol, such as sedation, ventilation, and anesthesia, and of the EEG recording conditions, such as the impedance of an electrode, fixation of a cap, the sampling frequency, and the field strength of the MRI scanner.

Impact of the α -chloralose anesthesia on neurovascular coupling

α -Chloralose is a commonly used anesthesia for rat fMRI studies due to its negligible cardiovascular effects. It results in a negligible change in the MABP and HR (Balis and Monroe, 1964), and more importantly, the evoked fMRI signals are well localized and larger than those of other anesthetics (Austin et al., 2005; Maandag et al.,

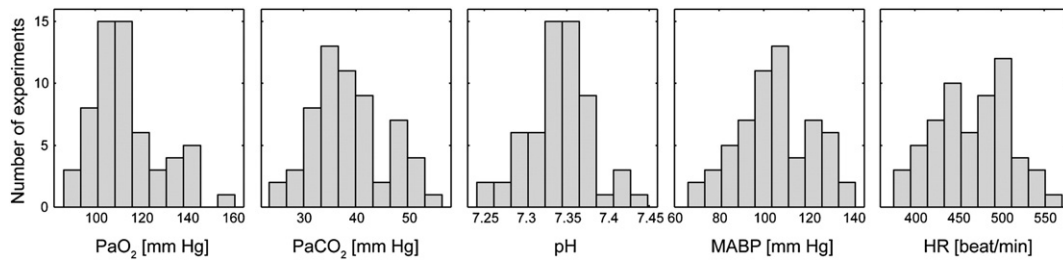


Fig. 5. Histograms of PaO₂, PaCO₂, pH, MABP, and HR. The x-axis denotes the actual value of each physiological parameter, and the y-axis denotes the number of experiments. These five physiological parameters were utilized for the multiple linear regression analysis.

2007). The pharmacological mechanisms of α -chloralose are still unclear, although it has been postulated that the anesthetic effect of α -chloralose may be mediated by its influence on GABAergic functions. The hypothesis is based on evidence that it can potentiate GABA-induced currents (Garrett and Gan, 1998). Given that fast-spiking GABAergic interneurons have a key role in neurovascular coupling (Cauli et al., 2004; Donahue et al., 2010) and in the generation of gamma oscillations (Cardin et al., 2009), the coupling between the gamma oscillation and fMRI signals could be enhanced under α -chloralose anesthesia, whereas that of lower frequency bands could be suppressed. This hypothesized enhancement is interpreted in relation to the study by Smith et al. (2002), in which the authors reported that the relative change in blood flow/volume and oxygen metabolism was highly dependent on the level of α -chloralose anesthesia, such that the deeper the α -chloralose anesthesia level, the higher the contrast in fMRI signal and spiking frequency. The latter-mentioned suppression was previously inferred by Lu et al. (2007), who demonstrated the α -chloralose anesthetic dose-dependent modulation of inter-hemispheric delta oscillations. They found that the deeper the α -chloralose anesthesia level, the lower the synchronization of inter-hemispheric delta oscillations. These inferences are further supported by Goense and Logothetis (2008), who found that all frequency bands, including the lower bands, were significantly correlated with fMRI signals in awake monkeys.

Coupling between gamma oscillations and fMRI signals

In a recent study, Kann et al. (2011) revealed that gamma oscillations are especially associated with higher mitochondrial oxidative metabolism, which is characterized by higher oxygen consumption and mitochondrial gene expression. These findings in particular help support the correlation between gamma oscillations and fMRI signals and why such a coupling is influenced by baseline physiological parameters. Some explanations may include the following: (1) fast-spiking GABAergic interneurons that contain large numbers of mitochondria with high cytochrome *c* levels are specifically involved in the generation of gamma oscillations (Gulyás et al., 2006); (2) fast alternating pairs of current sinks and sources during the gamma oscillations

Table 3

A summary of the results obtained from the multiple linear regression analysis between each Y_{data} and all of the physiological variables. The bold text indicates $p < 0.05$.

Y_{data}	Frequency band	R-squared	p-value
EEG (T-score)	delta (1–4 Hz)	0.347	0.000
	theta (4–8 Hz)	0.296	0.002
	alpha (8–12 Hz)	0.073	0.518
	beta (12–25 Hz)	0.074	0.513
	gamma (25–70 Hz)	0.080	0.460
fMRI (T-score)	–	0.078	0.480
Correlation coefficient between EEG and fMRI	delta (1–4 Hz)	0.324	0.001
	theta (4–8 Hz)	0.225	0.015
	alpha (8–12 Hz)	0.027	0.909
	beta (12–25 Hz)	0.037	0.836
	gamma (25–70 Hz)	0.200	0.029

require enhanced Na⁺/K⁺-ATPase activity to restore ionic gradients (Attwell and Iadecola, 2002); (3) local ATP consumption is rapidly counterbalanced through mitochondrial oxidative metabolism under a sufficient supply of glucose and O₂ (Cjedde et al., 2002); and (4) such a high energy demand cycle should be under the control of precise physiological balances in the cortical circuits. It has been previously demonstrated that neurovascular coupling is vulnerable to pathological conditions (Girouard and Iadecola, 2006) in which such precise control of physiology is almost exclusively disrupted. However, we note that these proposed interpretations cannot be extended to the resting-state in a straightforward manner, where the fMRI signals were differentially correlated with delta, theta, alpha, beta, and gamma oscillations, depending on the pattern of each brain network (Mantini et al., 2007b). Given that the gamma oscillations mostly contribute to local processing, such as sensory encoding (Donner and Siegel, 2011), we believe that the dependence of systemic physiological parameters on the more diverse oscillation pattern during rest should be dissimilar to the sensory-evoked state, which remains to be fully elucidated.

Distinct influence of the physiological parameter on neurovascular coupling

We considered three plausible reasons as to why the HR exhibits a significant contribution in neurovascular coupling: (1) the HR reflects the counterbalance of the autonomic nervous system, i.e., the sympathetic vs. the parasympathetic nervous system (Ramaekers et al., 2002), and more importantly, the sensitivity of the HR to the autonomic nervous system is generally more reliable than other physiological parameters; (2) the fluctuation of the HR is associated with a change in cardiac output, and therefore, can influence the basal cerebral blood flow; (3) the HR is an indicator of the depth of α -chloralose anesthesia and indicates that a light α -chloralose anesthesia level may induce enhanced coupling between the gamma oscillations and the fMRI signal. We consider (1) and (3) to be more plausible, because the cerebral blood flow and cardiac output are maintained at a constant level in the normal physiological range, even when the HR is controlled with a pace maker (Shapiro and Chawla, 1969). Meanwhile, both the pH and MABP exhibit a moderately significant contribution in neurovascular coupling. The increase/decrease of the pH (i.e., H⁺ ion) has a vessel dilation/constriction effect on the rat cerebral arterioles via changing of the membrane potential of vascular smooth muscle cells (Dietrich and Dacey, 1994). Therefore, the basal pH fluctuations may influence the

Table 4

The regression model for the correlation coefficient between the gamma band and fMRI signal. The bold text indicates $p < 0.05$.

	Coefficient	95% CI	p-value
Intercept (b_0)	–5.27	(–11.57, 1.03)	0.1
Regression slope for “PaO ₂ ” (b_{O_2})	0.00037	(–0.0016, 0.0023)	0.7
Regression slope for “PaCO ₂ ” (b_{CO_2})	–0.00067	(–0.0052, 0.0039)	0.8
Regression slope for “pH” (b_{pH})	0.78	(–0.036, 1.60)	0.06
Regression slope for “MABP” (b_{MABP})	–0.0014	(–0.0029, 0.00013)	0.07
Regression slope for “HR” (b_{HR})	0.00094	(0.00027, 0.0016)	0.007

basal cerebral blood flow or volume. The MABP also reflects the counterbalance of the autonomic nervous system and therefore is an indicator of the depth of α -chloralose anesthesia. However, the PaO₂ and PaCO₂ did not exhibit a significant contribution in neurovascular coupling within a normal physiological range, which is much narrower than the range in the studies using experimental interventions such as hypo/hyperoxia and hypo/hypercapnia. Therefore, we conclude that the impact of the PaO₂ and PaCO₂ is very limited within a normal physiological range compared with other systemic physiological parameters.

Limitations of the study and avenues for future research

1) In this study, we employed α -chloralose anesthesia, which may have confounded not only the EEG and fMRI results, but also the physiological parameters of the subjects. To more accurately extrapolate the results of this study to human cognitive fMRI studies, further experiments performed on awake animals (Lahti et al., 1998) will be required. These experiments should also validate the reproducibility of our conclusions. These studies should be performed both in the resting-state as well as under the event-related stimulation paradigm in awake animals.

2) It remains questionable whether fast-spiking GABAergic inhibitory neurons indeed play an indispensable role in the coupling between the gamma oscillations and fMRI signals and if there is a dependence on systemic physiological parameters. A pharmacological approach using a specific inhibitor for GABAergic interneurons would be insightful in future studies (e.g., GABA transaminase inhibitor, de Graaf et al., 2006), and a small animal model would allow the performance of such invasive interventions and simultaneous online monitoring of the physiological parameters.

3) We found that the HR demonstrates a statistically significant positive slope in multiple linear regression models, implying that the involvement of autonomic nervous system control is important in neurovascular coupling. Because the HR is thought to be an indirect output of the autonomic status of the subjects, we need to further confirm the impact of the autonomic system on neurovascular coupling using a more direct physiological index (Shmueli et al., 2007) such as cardiac pulsation, low/high frequency ratio of HR/BP variability, or plasma adrenaline levels.

Conclusions

In this study, we examined the trial-by-trial relationship between EEG and fMRI signals in the rat somatosensory cortex and their dependence on systemic parameters such as PaO₂, PaCO₂, pH, MABP, and HR within the normal physiological range. Our main findings are as follows: (1) the power of the gamma oscillations demonstrates maximum correlation with the fMRI signal; (2) the correlation coefficient between the power in the gamma range and fMRI signal is statistically explained by the physiological parameters; (3) the fMRI signal and the power of the gamma band in the EEG signal itself are independent; and (4) among the physiological parameters, the HR shows a statistically significant positive slope in the multiple linear regression model. The respiratory effect and cardiac pulsatility have been considered to be sources of physiological noise in human fMRI studies, and several retrospective correction methods for these artifacts have been developed (Birn et al., 2008; Chang et al., 2009; Deckers et al., 2006; Glover et al., 2000). Thus, the influence of physiological noise on fMRI signals has been eliminated with these methods. Elimination enhances the cognitive fMRI features; however, given the characteristics of the fMRI contrast, the fMRI method will provide important information on the relationship between brain function and physiology. Clearly, more studies are needed to investigate the outstanding questions raised in this study; however, we expect that our findings will provide fundamental guidance when interpreting the

dependence of the EEG, fMRI, or the coupling data on physiological parameters in human or animal subjects.

Acknowledgments

The authors would like to thank Ms. Sarah Michael for her careful revision of the manuscript, Mr. Hiroi Nonaka for his technical assistance, and all of our colleagues at Tohoku University for their tremendous support.

Appendix A. Supplementary data

Supplementary data to this article can be found online at doi:10.1016/j.neuroimage.2011.12.082.

References

- Attwell, D., Iadecola, C., 2002. The neural basis of functional brain imaging signals. *Trends Neurosci.* 25, 621–625.
- Austin, V.C., Blamire, A.M., Allers, K.A., Sharp, T., Styles, P., Matthews, P.M., Sibson, N.R., 2005. Confounding effects of anesthesia on functional activation in rodent brain: a study of halothane and α -chloralose anesthesia. *NeuroImage* 24, 92–100.
- Balis, G.U., Monroe, R.R., 1964. The pharmacology of chloralose. A review. *Psychopharmacologia* 6, 1–30.
- Bandettini, P.A., 2009. Seven topics in functional magnetic resonance imaging. *J. Integr. Neurosci.* 8, 371–403.
- Bénar, C., Aghakhani, Y., Wang, Y., Izenberg, A., Al-Asmi, A., Dubeau, F., Gotman, J., 2003. Quality of EEG in simultaneous EEG–fMRI for epilepsy. *Clin. Neurophysiol.* 114, 569–580.
- Birn, R.M., Smith, M.A., Jones, T.B., Bandettini, P.A., 2008. The respiration response function: the temporal dynamics of fMRI signal fluctuations related to changes in respiration. *NeuroImage* 40, 644–654.
- Buxton, R.B., 2002. Introduction to Functional Magnetic Resonance Imaging: Principles and Techniques. Cambridge University Press.
- Cardin, J.A., Carlén, M., Meletis, K., Knoblich, U., Zhang, F., Deisseroth, K., Tsai, L.H., Moore, C.L., 2009. Driving fast-spiking cells induces gamma rhythm and controls sensory responses. *Nature* 459, 663–667.
- Cauli, B., Tong, X.K., Rancillac, A., Serluca, N., Lambolez, B., Rossier, J., Hamel, E., 2004. Cortical GABA interneurons in neurovascular coupling: relays for subcortical vasoactive pathways. *J. Neurosci.* 24, 8940–8949.
- Chang, C., Cunningham, J.P., Glover, G.H., 2009. Influence of heart rate on the BOLD signal: the cardiac response function. *NeuroImage* 44, 857–869.
- Chiarelli, P.A., Bulte, D.P., Wise, R., Gallichan, D., Jezzard, P., 2007. A calibration method for quantitative BOLD fMRI based on hyperoxia. *NeuroImage* 37, 808–820.
- Corfield, D.R., Murphy, K., Josephs, O., Adams, L., Turner, R., 2001. Does hypercapnia-induced cerebral vasodilation modulate the hemodynamic response to neural activation? *NeuroImage* 13, 1207–1211.
- de Graaf, R.A., Patel, A.B., Rothman, D.L., Behar, K.L., 2006. Acute regulation of steady-state GABA levels following GABA-transaminase inhibition in rat cerebral cortex. *Neurochem. Int.* 48, 508–514.
- Debener, S., Thorne, J., Schneider, T.R., Viola, F.C., 2010. Using ICA for the analysis of multi-channel EEG data. In: Ullsperger, M., Debener, S. (Eds.), *Simultaneous EEG and fMRI: Recording, Analysis, and Application*. Oxford University Press, pp. 121–133.
- Deckers, R.H.R., van Gelderen, P., Ries, M., Barret, O., Duyn, J.H., Ikonomidou, V.N., Fukunaga, M., Glover, G.H., de Zwart, J.A., 2006. An adaptive filter for suppression of cardiac and respiratory noise in MRI time series data. *NeuroImage* 33, 1072–1081.
- Dietrich, H.H., Dacey, R.G., 1994. Effects of extracellular acidification and extravascular alkalization on constriction and depolarization in rat cerebral arterioles in vitro. *J. Neurosurg.* 81, 437–442.
- Donahue, M.J., Near, J., Blicher, J.U., Jezzard, P., 2010. Baseline GABA concentration and fMRI response. *NeuroImage* 53, 392–398.
- Donner, T.H., Siegel, M., 2011. A framework for local cortical oscillation patterns. *Trends Cogn. Sci.* 15, 191–199.
- Franceschini, M.A., Radhakrishnan, H., Thakur, K., Wu, W., Ruvinskaya, S., Carp, S., Boas, D.A., 2010. The effect of different anesthetics on neurovascular coupling. *NeuroImage* 51, 1367–1377.
- Friston, K.J., 2009. Modalities, modes, and models in functional neuroimaging. *Science* 326, 399–403.
- Garrett, K.M., Gan, J., 1998. Enhancement of γ -aminobutyric acid_A receptor activity by α -chloralose. *J. Pharmacol. Exp. Ther.* 285, 680–686.
- Girouard, H., Iadecola, C., 2006. Neurovascular coupling in the normal brain and in hypertension, stroke, and Alzheimer disease. *J. Appl. Physiol.* 100, 328–335.
- Gjedde, A., Marrett, S., Vafaee, M., 2002. Oxidative and nonoxidative metabolism of excited neurons and astrocytes. *J. Cereb. Blood Flow Metab.* 22, 1–14.
- Glover, G.H., Li, T.Q., Ress, D., 2000. Image-based method for retrospective correction of physiological motion effects in fMRI: RETROICOR. *Magn. Reson. Med.* 44, 162–167.
- Goense, J.B.M., Logothetis, N.K., 2008. Neurophysiology of the BOLD fMRI signal in awake monkeys. *Curr. Biol.* 18, 631–640.

- Gulyás, A.I., Buzsáki, G., Freund, T.F., Hirase, H., 2006. Populations of hippocampal inhibitory neurons express different levels of cytochrome c. *Eur. J. Neurosci.* 23, 2581–2594.
- He, B.J., Snyder, A.Z., Zempel, J.M., Smyth, M.D., Raichle, M.E., 2008. Electrophysiological correlates of the brain's intrinsic large-scale functional architecture. *Proc. Natl. Acad. Sci. U. S. A.* 105, 16039–16044.
- Huttunen, J.K., Gröhn, O., Penttonen, M., 2008. Coupling between simultaneously recorded BOLD response and neuronal activity in the rat somatosensory cortex. *NeuroImage* 39, 775–785.
- Hyder, F., Behar, K.L., Martin, M.A., Blamire, A.M., Shulman, R.G., 1994. Dynamic magnetic resonance imaging of the rat brain during forepaw stimulation. *J. Cereb. Blood Flow Metab.* 14, 649–655.
- Jezzard, P., Rauschecker, J.P., Malonek, D., 1997. An *in vivo* model for functional MRI in cat visual cortex. *Magn. Reson. Med.* 38, 699–705.
- Jung, T.P., Makeig, S., Westerfield, M., Townsend, J., Courchesne, E., Sejnowski, T.J., 2001. Analysis and visualization of single-trial event-related potentials. *Hum. Brain Mapp.* 14, 166–185.
- Kann, O., Huchzermeyer, C., Kovács, R., Wirtz, S., Schuelke, M., 2011. Gamma oscillations in the hippocampus require high complex I gene expression and strong functional performance of mitochondria. *Brain* 134, 345–358.
- Lachaux, J.P., Fonlupt, P., Kahane, P., Minotti, L., Hoffmann, D., Bertrand, O., Bacia, M., 2007. Relationship between task-related gamma oscillations and BOLD signal: new insights from combined fMRI and intracranial EEG. *Hum. Brain Mapp.* 28, 1368–1375.
- Lahti, K.M., Ferris, C.F., Li, F., Sotak, C.H., King, J.A., 1998. Imaging brain activity in conscious animals using functional MRI. *J. Neurosci. Methods* 82, 75–83.
- Levin, J.M., Frederick, B.B., Ross, M.H., Fox, J.F., von Rosenberg, H.L., Kaufman, M.J., Lange, N., Mendelson, J.H., Cohen, B.M., Renshaw, P.F., 2001. Influence of baseline hematocrit and hemodilution on BOLD fMRI activation. *Magn. Reson. Imaging* 19, 1055–1062.
- Lin, W., Paczynski, R.P., Celik, A., Hsu, C.Y., Powers, W.J., 1998. Effects of acute normovolemic hemodilution on T_2^* -weighted images of rat brain. *Magn. Reson. Med.* 40, 857–864.
- Logothetis, N.K., 2008. What we can do and what we cannot do with fMRI. *Nature* 453, 869–878.
- Logothetis, N.K., Guggenberger, H., Peled, S., Pauls, J., 1999. Functional imaging of the monkey brain. *Nat. Neurosci.* 2, 555–562.
- Logothetis, N.K., Pauls, J., Augath, M., Trinath, T., Oeltermann, A., 2001. Neurophysiological investigation of the basis of the fMRI signal. *Nature* 412, 150–157.
- Lu, H., Zuo, Y., Gu, H., Waltz, J.A., Zhan, W., Scholl, C.A., Rea, W., Yang, Y., Stein, E.A., 2007. Synchronized delta oscillations correlate with the resting-state functional MRI signal. *Proc. Natl. Acad. Sci. U. S. A.* 104, 18265–18269.
- Maandag, N.J.G., Coman, D., Sanganahalli, B.G., Herman, P., Smith, A.J., Blumenfeld, H., Shulman, R.G., Hyder, F., 2007. Energetics of neuronal signaling and fMRI activity. *Proc. Natl. Acad. Sci. U. S. A.* 104, 20546–20551.
- Mantini, D., Perrucci, M.G., Cugini, S., Ferretti, A., Romani, G.L., Del Gratta, C., 2007a. Complete artifact removal for EEG recorded during continuous fMRI using independent component analysis. *NeuroImage* 34, 598–607.
- Mantini, D., Perrucci, M.G., Del Gratta, C., Romani, G.L., Corbetta, M., 2007b. Electrophysiological signatures of resting state networks in the human brain. *Proc. Natl. Acad. Sci. U. S. A.* 104, 13170–13175.
- Masamoto, K., Vazquez, A., Wang, P., Kim, S., 2008. Trial-by-trial relationship between neural activity, oxygen consumption, and blood flow responses. *NeuroImage* 40, 442–450.
- Mukamel, R., Gelbard, H., Arieli, A., Hasson, U., Fried, I., Malach, R., 2005. Coupling between neuronal firing, field potentials, and fMRI in human auditory cortex. *Science* 309, 951–954.
- Nakamura, W., Anami, K., Mori, T., Saitoh, O., Cichocki, A., Amari, S., 2006. Removal of ballistocardiogram artifacts from simultaneously recorded EEG and fMRI data using independent component analysis. *IEEE Trans. Biomed. Eng.* 53, 1294–1308.
- Niessing, J., Ebisch, B., Schmidt, K.E., Niessing, M., Singer, W., Galuske, R.A.W., 2005. Hemodynamic signals correlate tightly with synchronized gamma oscillations. *Science* 309, 948–951.
- Nir, Y., Fisch, L., Mukamel, R., Gelbard-Sagiv, H., Arieli, A., Fried, I., Malach, R., 2007. Coupling between neuronal firing rate, gamma LFP, and BOLD fMRI is related to inter-neuronal correlations. *Curr. Biol.* 17, 1275–1285.
- Posse, S., Kemna, L.J., Elghahwagi, B., Wiese, S., Kiselev, V.G., 2001. Effect of graded hypo- and hypercapnia on fMRI contrast in visual cortex: quantification of T_2^* changes by multiecho EPI. *Magn. Reson. Med.* 46, 264–271.
- Qiao, M., Rushforth, D., Wang, R., Shaw, R.A., Tomanek, B., Dunn, J.F., Tuor, U.J., 2007. Blood-oxygen-level-dependent magnetic resonance signal and cerebral oxygenation responses to brain activation are enhanced by concurrent transient hypertension in rats. *J. Cereb. Blood Flow Metab.* 27, 1280–1289.
- Ramaekers, D., Beckers, F., Demeulemeester, H., Aubert, A.E., 2002. Cardiovascular autonomic function in conscious rats: a novel approach to facilitate stationary conditions. *Ann. Noninvasive Electrocardiol.* 7, 307–318.
- Riera, J.J., Sumiyoshi, A., 2010. Brain oscillations: ideal scenery to understand the neurovascular coupling. *Curr. Opin. Neurol.* 23, 374–381.
- Scheeringa, R., Fries, P., Petersson, K.M., Oostenveld, R., Grothe, I., Norris, D.G., Hagoort, P., Bastiaansen, M.C.M., 2011. Neuronal dynamics underlying high- and low-frequency EEG oscillations contribute independently to the human BOLD signal. *Neuron* 69, 572–583.
- Schölvinck, M.L., Maier, A., Ye, F.Q., Duyn, J.H., Leopold, D.A., 2010. Neural basis of global resting-state fMRI activity. *Proc. Natl. Acad. Sci. U. S. A.* 107, 10238–10243.
- Shapiro, W., Chawla, N.P., 1969. Observations on the regulation of cerebral blood flow in complete heart block. *Circulation* 40, 863–870.
- Shmueli, K., van Gelderen, P., de Zwart, J.A., Horowitz, S.G., Fukunaga, M., Jansma, J.M., Duyn, J.H., 2007. Low-frequency fluctuations in the cardiac rate as a source of variance in the resting-state fMRI BOLD signal. *NeuroImage* 38, 306–320.
- Sicard, K.M., Duong, T.Q., 2005. Effects of hypoxia, hyperoxia, and hypercapnia on baseline and stimulus-evoked BOLD, CBF, and CMRO₂ in spontaneously breathing animals. *NeuroImage* 25, 850–858.
- Smith, A.J., Blumenfeld, H., Behar, K.L., Rothman, D.L., Shulman, R.G., Hyder, F., 2002. Cerebral energetics and spiking frequency: the neurophysiological basis of fMRI. *Proc. Natl. Acad. Sci. U. S. A.* 99, 10765–10770.
- Sohal, V.S., Zhang, F., Yizhar, O., Deisseroth, K., 2009. Parvalbumin neurons and gamma rhythms enhance cortical circuit performance. *Nature* 459, 698–702.
- Srivastava, G., Crottaz-Herbette, S., Lau, K.M., Glover, G.H., Menon, V., 2005. ICA-based procedures for removing ballistocardiogram artifacts from EEG data acquired in the MRI scanner. *NeuroImage* 24, 50–60.
- Steward, C.A., Marsden, C.A., Prior, M.J.W., Morris, P.G., Shah, Y.B., 2005. Methodological considerations in rat brain BOLD contrast pharmacological MRI. *Psychopharmacology (Berl)* 180, 687–704.
- Sumiyoshi, A., Riera, J.J., Ogawa, T., Kawashima, R., 2011. A mini-cap for simultaneous EEG and fMRI recording in rodents. *NeuroImage* 54, 1951–1965.
- Traub, R.D., Whittington, M.A., Stanford, I.M., Jefferys, J.G., 1996. A mechanism for generation of long-range synchronous fast oscillations in the cortex. *Nature* 383, 621–624.
- Vanderperren, K., De Vos, M., Ramautar, J.R., Novitskiy, N., Mennes, M., Asseconci, S., Vanrumste, B., Stiers, P., Van den Bergh, B.R.H., Wagemans, J., Lagae, L., Sunaert, S., Van Huffel, S., 2010. Removal of BCG artifacts from EEG recordings inside the MR scanner: a comparison of methodological and validation-related aspects. *NeuroImage* 50, 920–934.
- Villringer, A., Mulert, C., Lemieux, L., 2010. Principles of multimodal functional imaging and data integration. In: Mulert, C., Lemieux, L. (Eds.), *EEG–fMRI: Physiological Basis, Technique and Application*. Springer, pp. 3–17.
- Viswanathan, A., Freeman, R.D., 2007. Neurometabolic coupling in cerebral cortex reflects synaptic more than spiking activity. *Nat. Neurosci.* 10, 1308–1312.
- Wibral, M., Muckli, L., Melnikovic, K., Scheller, B., Alink, A., Singer, W., Munk, M.H., 2007. Time-dependent effects of hyperoxia on the BOLD fMRI signal in primate visual cortex and LGN. *NeuroImage* 35, 1044–1063.
- Zappe, A.C., Uludağ, K., Logothetis, N.K., 2008. Direct measurement of oxygen extraction with fMRI using 6% CO₂ inhalation. *Magn. Reson. Imaging* 26, 961–967.